

itself into the LBP. Interestingly this orientation is the same as that of 6 $\alpha$ -ethyl-chenodeoxycholic acid (6 $\alpha$ -ethyl-CDCA) in the farnesoid X receptor (FXR) (36). LCA and its derivatives are similar in size (14–16 Å  $\times$  5 Å  $\times$  3 Å; length  $\times$  width  $\times$  thickness) to natural 1,25(OH) $_2$ D $_3$  (approximately 15 Å  $\times$  5 Å  $\times$  2 Å), and although their shapes are somewhat different, the nonplanar *cis* A/B rings of the steroid scaffold of LCA mimic the curvature of the 9,10-secosteroid portion of 1,25(OH) $_2$ D $_3$  (Fig. 3C). Often, the size seems to be critical to the agonistic activity of a ligand. Agonistic ligands induce a conformational change of loop 11–12 to bring helix 12 into the active conformation, which is stabilized by hydrophobic interactions between the ligand and Val418 and Phe422 (Val414 and Phe418 of rat VDR, respectively). This conformation creates the AF-2 surface and allows the coactivator to bind, which is required for the VDR activity. Large ligands could collide with helix 12 and destabilize the active conformation. Indeed, several larger ligands have been reported to show antagonistic activity instead of agonistic activity (32, 37).

Despite their opposite orientation, LCA and its derivatives can reproduce the interactions between VDR and 1,25(OH) $_2$ D $_3$ , which consists of a hydrophobic secosteroid framework and three polar groups. The polar groups are located at the both ends of the ligand and stabilize ligand binding through several hydrogen bonds, while the hydrophobic secosteroid frame just fits the hydrophobic tunnel of the LBP. In the complex with 1,25(OH) $_2$ D $_3$ , the A-ring of 1,25(OH) $_2$ D $_3$  deeply wedges itself into the LBP and its 25-hydroxyl group is set on the inlet of the LBP. There are two polar groups at the C-1 and C-3 positions of the A-ring of 1,25(OH) $_2$ D $_3$ , whose oxygen atoms form two pairs of bifurcated hydrogen bonds with the side chains of Tyr143 and Ser274, and Ser233 and Arg270, respectively. Furthermore, the 25-hydroxyl group of 1,25(OH) $_2$ D $_3$  also forms a bifurcated hydrogen bond with the nitrogen atoms of the imidazole rings of His301 and His393. In contrast, LCA and its derivatives consist of the hydrophobic steroid framework and two polar groups at the both ends (Fig. 1). However, they maintain most of the hydrogen bonds between the ligand and the protein by exchanging the hydrogen-bonding partners between the A-ring and the carboxyl group. Two oxygen atoms of the 24-carboxyl group form, with the help of a water molecule, two pairs of bifurcated hydrogen bonds directly with the side chains of Tyr143 and Ser274, and indirectly with Ser233 and Arg270, respectively. The hydrogen bonds with the nitrogen atoms of the imidazole rings of His301 and His393 are partially formed, depending on the substituents at the C-3 position of the A-ring. Therefore, the hydrogen-bonding network between the ligand and the protein is essentially the same for both LCA and 1,25(OH) $_2$ D $_3$ , even though their orientations are opposite. Adachi et al. also indicated the importance of the hydrogen-bonding network for agonistic activity by showing that esterification of the carboxyl group of LCA weakened its agonistic activity (18).

Although LCA mimicked the dimensions and chemical properties of 1,25(OH) $_2$ D $_3$  as discussed above, its affinity is much lower than 1,25(OH) $_2$ D $_3$ . In a competitive binding

assay using VDR fused to glutathione S-transferase, IC $_{50}$  values were estimated as 0.08 nM and 300  $\mu$ M for 1,25(OH) $_2$ D $_3$  and LCA, respectively (19). As the accessible surface areas of the hydrophobic surface of LCA and 1,25(OH) $_2$ D $_3$  are 371 Å $^2$  and 442 Å $^2$ , respectively, the total hydrophobic interaction of LCA with VDR would be expected to be smaller than that of 1,25(OH) $_2$ D $_3$ . Also the simple difference of the size between LCA (C $_{24}$ H $_{40}$ O $_3$ ) and 1,25(OH) $_2$ D $_3$  (C $_{27}$ H $_{44}$ O $_3$ ) suggests that the LBP accommodates LCA somewhat loosely. Such a feature allows several water molecules to penetrate the LBP of VDR. One of the water molecules is involved in the hydrogen bond network around the 24-carboxyl group. Another water molecule is incorporated in the hydrogen bond network around the C-3 position of the A-ring in the complex with LCA. However, given the affinity analyses mentioned above, the interactions mediated by hydrogen bonding seem to be less important for stabilizing the complex than the hydrophobic interactions.

The substituents at the C-3 position of the A-ring of LCA also affect the activation of human VDR, and LCA acetate and LCA propionate are more potent agonists than LCA and 3-keto LCA (18, 19, 22, 38). The binding assay mentioned above showed that IC $_{50}$  values for LCA acetate and LCA propionate are 30  $\mu$ M, about 10 times more potent than LCA (19). Another cotransfection assay showed LCA acetate (EC $_{50}$  = 0.40  $\mu$ M) is about 30 times more effective than LCA (EC $_{50}$  = 12.1  $\mu$ M), whereas 3-keto LCA (EC $_{50}$  = 6.8  $\mu$ M) is comparable to LCA (18). Our crystal structures show that the C-3 substituents of the former derivatives interact directly with VDR via a hydrogen bond, while the latter ones require a water molecule to form indirect hydrogen bonds with VDR. In addition, the alkyl part of these acyl groups interacts with the hydrophobic residues of VDR, including Val418 and Phe422 (Val414 and Phe418 of rat VDR, respectively), which are key residues in the VDR activation mechanism described above. These interactions are probably the reason for the higher potency of these two ligands because this valine is not directly involved in the interaction with the ligands in the case of LCA and 3-keto LCA. These additional interactions at the C-3 position may also explain some of the mutation analyses; the human VDR-S275A and S278A mutations (corresponding to S271A and S274A of rat VDR, respectively) almost completely abolished the activity of LCA, whereas they were still activated by LCA acetate (18). The extra interactions at the C-3 position compensate for the loss of the hydrogen bond due to the mutation to some extent.

Some of the other results from the mutation analyses could also be explained from our structure (18, 19, 22, 38). The VDR-S237M mutant (S233M of rat VDR) can respond to LCA but not to 1,25(OH) $_2$ D $_3$ . The serine residue directly interacts with the A-ring of 1,25(OH) $_2$ D $_3$  through a hydrogen bond, and the mutation to methionine would not only lose the capability of the interaction but also hinder the ligand binding. On the other hand, the bulky A-ring is replaced by a linear alkyl group in LCA (Fig. 3C), creating enough room to accommodate in the methionine. In contrast, the VDR-S278V mutant (S274V of rat VDR) is



activated by  $1,25(\text{OH})_2\text{D}_3$  but not by LCA. The side chain of the serine also directly interacts with the hydroxyl group of the A-ring of  $1,25(\text{OH})_2\text{D}_3$  and the carboxyl group of LCA. The mutation to valine would lose the hydrogen bond, but there is enough room to accommodate the replaced side chain in both cases. LCA might disfavor the mutant that would bring the hydrophobic valine close to the negative charge of the carboxyl group.


The role of His305 (His301 of rat VDR) in the interactions with the LCA-related ligands seems more complicated. Although LCA and 3-keto LCA interact with His305 in a very similar manner (Fig. 3A), the VDR-H305A (H301A of rat VDR) mutant significantly diminishes the LCA activity but has little effect on activation by LCA acetate or 3-keto LCA. The indole ring lies almost parallel to the A-ring of LCA, making van der Waals contacts. It is also involved in the hydrogen bond directly (LCA acetate) or indirectly (LCA and 3-keto LCA). These interactions are almost the only interactions between the ligand and loop 6–7, and the mutation to alanine may perhaps trigger a large conformational change of the loop, which could even expose the ligand to the solvent.

Although LCA activates VDR, it functions differently from  $1,25(\text{OH})_2\text{D}_3$ ; for example, it does not induce hypercalcemia. The most prominent difference in the ligand binding between  $1,25(\text{OH})_2\text{D}_3$  and the LCA-related ligands reported here are the pattern of the hydrogen bonds with Ser233 in helix 3 and Arg270 in helix 4/5. While  $1\alpha$ -hydroxyl group of  $1,25(\text{OH})_2\text{D}_3$  directly forms the hydrogen bonds with these two residues, all the LCA-related ligands studied here require a water molecule to form indirect hydrogen bonds with them, which is likely to weaken the interaction with VDR. Also, replacing the A-ring of  $1,25(\text{OH})_2\text{D}_3$  with a linear alkyl group seems to loosen the hydrophobic interactions around it, as highlighted by the VDR-S237M mutant discussed above. These differences may affect the structure of the AF-2 surface and, therefore, the interactions between VDR and the coactivators statically and/or dynamically.

However, we did not detect significant differences in the interactions between VDR and the coactivator peptide. One possible reason is the crystal packing. The coactivator peptide not only interacts with VDR but also plays an important role in the crystal packing, and even antagonists could be trapped in its active form at high concentrations as in the crystallization conditions (32). Thus the structural differences that may be caused by LCA could have been suppressed by the crystal packing. The possibility that LCA behaves differently from  $1,25(\text{OH})_2\text{D}_3$  through a nonstructural mechanism also cannot be excluded. Their metabolic behavior and/or cellular distribution would be different in vivo, causing the functional differences. To rationally elucidate the underlying reason for the difference in the agonistic activity between the ligands, it will be necessary to analyze the higher-ordered complexes, perhaps using full-length VDR. The crystal structures reported here nonetheless have shown the similarities and differences between LCA-related ligands and  $1,25(\text{OH})_2\text{D}_3$  in their interactions with VDR and should provide a sound

basis for the design of new ligands based on LCA, hopefully with better pharmaceutical features.

#### Data deposition

The coordinates of the determined structures have been deposited in the Protein Data Bank with accession numbers 3W5P, 3W5Q, 3W5R, and 3W5T for the LCA, 3keto-LCA, LCA acetate, and LCA propionate complexes, respectively. 

The authors thank Professor H. Kagechika and Professor H. Tamamura of Tokyo Medical and Dental University for supporting this research project. The authors also thank the technical staff at the Photon Factory of the High Energy Accelerator Research Organization for maintenance of the beam line.

#### REFERENCES

1. Haussler, M. R., G. K. Whitfield, C. A. Haussler, J. C. Hsieh, P. D. Thompson, S. H. Selznick, C. E. Dominguez, and P. W. Jurutka. 1998. The nuclear vitamin D receptor: biological and molecular regulatory properties revealed. *J. Bone Miner. Res.* **13**: 325–349.
2. Abe, E., C. Miyaura, H. Sakagami, M. Takeda, K. Konno, T. Yamazaki, S. Yoshiki, and T. Suda. 1981. Differentiation of mouse myeloid leukemia cells induced by  $1\alpha,25$ -dihydroxyvitamin  $\text{D}_3$ . *Proc. Natl. Acad. Sci. USA*. **78**: 4990–4994.
3. DeLuca, H. F. 2004. Overview of general physiologic features and functions of vitamin D. *Am. J. Clin. Nutr.* **80**(Suppl.): 1689–1696.
4. Hosomi, J., J. Hosoi, E. Abe, T. Suda, and T. Kuroki. 1983. Regulation of terminal differentiation of cultured mouse epidermal cells by  $1\alpha,25$ -dihydroxyvitamin  $\text{D}_3$ . *Endocrinology*. **113**: 1950–1957.
5. Lemire, J. M. 1992. Immunomodulatory role of  $1,25$ -dihydroxyvitamin  $\text{D}_3$ . *J. Cell. Biochem.* **49**: 26–31.
6. Smith, E. L., N. C. Walworth, and M. F. Holick. 1986. Effect of  $1\alpha,25$ -dihydroxyvitamin  $\text{D}_3$  on the morphologic and biochemical differentiation of cultured human epidermal keratinocytes grown in serum-free conditions. *J. Invest. Dermatol.* **86**: 709–714.
7. Tanaka, H., E. Abe, C. Miyaura, T. Kuribayashi, K. Konno, Y. Nishii, and T. Suda. 1982.  $1\alpha,25$ -Dihydroxycholecalciferol and a human myeloid leukaemia cell line (HL-60). *Biochem. J.* **204**: 713–719.
8. Bortman, P., M. A. Folgueira, M. L. Katayama, I. M. Snitcovsky, and M. M. Brentani. 2002. Antiproliferative effects of  $1,25$ -dihydroxyvitamin  $\text{D}_3$  on breast cells: a mini review. *Braz. J. Med. Biol. Res.* **35**: 1–9.
9. Fraser, D., S. W. Kooh, H. P. Kind, M. F. Holick, Y. Tanaka, and H. F. DeLuca. 1973. Pathogenesis of hereditary vitamin-D-dependent rickets. An inborn error of vitamin D metabolism involving defective conversion of  $25$ -hydroxyvitamin D to  $1\alpha,25$ -dihydroxyvitamin D. *N. Engl. J. Med.* **289**: 817–822.
10. Glorieux, F. H., P. J. Marie, J. M. Pettifor, and E. E. Delvin. 1980. Bone response to phosphate salts, ergocalciferol, and calcitriol in hypophosphatemic vitamin D-resistant rickets. *N. Engl. J. Med.* **303**: 1023–1031.
11. Hayes, C. E. 2000. Vitamin D: a natural inhibitor of multiple sclerosis. *Proc. Nutr. Soc.* **59**: 531–535.
12. Konety, B. R., and R. H. Getzenberg. 2002. Vitamin D and prostate cancer. *Urol. Clin. North Am.* **29**: 95–106, ix.
13. Lambert-Allardt, C. 1991. Is there a role for vitamin D in osteoporosis? *Calcif. Tissue Int.* **49**(Suppl.): S46–S49.
14. Langner, A., H. Verjans, V. Stapor, M. Mol, and M. Fraczykowska. 1993. Topical calcitriol in the treatment of chronic plaque psoriasis: a double-blind study. *Br. J. Dermatol.* **128**: 566–571.
15. Yamada, S., M. Shimizu, and K. Yamamoto. 2003. Vitamin D receptor. *Endocr. Dev.* **6**: 50–68.
16. Bouillon, R., W. H. Okamura, and A. W. Norman. 1995. Structure-function relationships in the vitamin D endocrine system. *Endocr. Rev.* **16**: 200–257.
17. Boehm, M. F., P. Fitzgerald, A. Zou, M. G. Elgort, E. D. Bischoff, L. Merc, D. E. Mais, R. P. Bissonnette, R. A. Heyman, A. M. Nadzan, et al. 1999. Novel nonsecosteroidal vitamin D mimics exert



- VDR-modulating activities with less calcium mobilization than 1,25-dihydroxyvitamin D<sub>3</sub>. *Chem. Biol.* **6**: 265–275.
18. Adachi, R., Y. Honma, H. Masuno, K. Kawana, I. Shimomura, S. Yamada, and M. Makishima. 2005. Selective activation of vitamin D receptor by lithocholic acid acetate, a bile acid derivative. *J. Lipid Res.* **46**: 46–57.
  19. Ishizawa, M., M. Matsunawa, R. Adachi, S. Uno, K. Ikeda, H. Masuno, M. Shimizu, K. Iwasaki, S. Yamada, and M. Makishima. 2008. Lithocholic acid derivatives act as selective vitamin D receptor modulators without inducing hypercalcemia. *J. Lipid Res.* **49**: 763–772.
  20. Makishima, M., T. T. Lu, W. Xie, G. K. Whitfield, H. Domoto, R. M. Evans, M. R. Haussler, and D. J. Mangelsdorf. 2002. Vitamin D receptor as an intestinal bile acid sensor. *Science*. **296**: 1313–1316.
  21. Degirolamo, C., S. Modica, G. Palasciano, and A. Moschetta. 2011. Bile acids and colon cancer: solving the puzzle with nuclear receptors. *Trends Mol. Med.* **17**: 564–572.
  22. Choi, M., K. Yamamoto, T. Itoh, M. Makishima, D. J. Mangelsdorf, D. Moras, H. F. DeLuca, and S. Yamada. 2003. Interaction between vitamin D receptor and vitamin D ligands: two-dimensional alanine scanning mutational analysis. *Chem. Biol.* **10**: 261–270.
  23. Ciesielski, F., N. Rochel, A. Mitschler, A. Kouzmenko, and D. Moras. 2004. Structural investigation of the ligand binding domain of the zebrafish VDR in complexes with 1 $\alpha$ ,25(OH)<sub>2</sub>D<sub>3</sub> and Gemini: purification, crystallization and preliminary X-ray diffraction analysis. *J. Steroid Biochem. Mol. Biol.* **89–90**: 55–59.
  24. Eelen, G., L. Verlinden, N. Rochel, F. Claessens, P. De Clercq, M. Vandewalle, G. Tocchini-Valentini, D. Moras, R. Bouillon, and A. Verstuyf. 2005. Superagonistic action of 14-epi-analogs of 1,25-dihydroxyvitamin D explained by vitamin D receptor-coactivator interaction. *Mol. Pharmacol.* **67**: 1566–1573.
  25. Hourai, S., T. Fujishima, A. Kittaka, Y. Suhara, H. Takayama, N. Rochel, and D. Moras. 2006. Probing a water channel near the A-ring of receptor-bound 1  $\alpha$ ,25-dihydroxyvitamin D<sub>3</sub> with selected 2  $\alpha$ -substituted analogues. *J. Med. Chem.* **49**: 5199–5205.
  26. Rochel, N., S. Hourai, X. Perez-Garcia, A. Rumbo, A. Mourino, and D. Moras. 2007. Crystal structure of the vitamin D nuclear receptor ligand binding domain in complex with a locked side chain analog of calcitriol. *Arch. Biochem. Biophys.* **460**: 172–176.
  27. Rochel, N., J. M. Wurtz, A. Mitschler, B. Klaholz, and D. Moras. 2000. The crystal structure of the nuclear receptor for vitamin D bound to its natural ligand. *Mol. Cell.* **5**: 173–179.
  28. Shimizu, M., Y. Miyamoto, H. Takaku, M. Matsuo, M. Nakabayashi, H. Masuno, N. Udagawa, H. F. DeLuca, T. Ikura, and N. Ito. 2008. 2-Substituted-16-ene-22-thia-1 $\alpha$ ,25-dihydroxy-26,27-dimethyl-19-norvitamin D<sub>3</sub> analogs: synthesis, biological evaluation, and crystal structure. *Bioorg. Med. Chem.* **16**: 6949–6964.
  29. Tocchini-Valentini, G., N. Rochel, J. M. Wurtz, A. Mitschler, and D. Moras. 2001. Crystal structures of the vitamin D receptor complexed to superagonist 20-epi ligands. *Proc. Natl. Acad. Sci. USA*. **98**: 5491–5496.
  30. Tocchini-Valentini, G., N. Rochel, J. M. Wurtz, and D. Moras. 2004. Crystal structures of the vitamin D nuclear receptor liganded with the vitamin D side chain analogues calcipotriol and seocalcitrol, receptor agonists of clinical importance. Insights into a structural basis for the switching of calcipotriol to a receptor antagonist by further side chain modification. *J. Med. Chem.* **47**: 1956–1961.
  31. Vanhooke, J. L., M. M. Benning, C. B. Bauer, J. W. Pike, and H. F. DeLuca. 2004. Molecular structure of the rat vitamin D receptor ligand binding domain complexed with 2-carbon-substituted vitamin D<sub>3</sub> hormone analogues and a LXXLL-containing coactivator peptide. *Biochemistry*. **43**: 4101–4110.
  32. Nakabayashi, M., S. Yamada, N. Yoshimoto, T. Tanaka, M. Igarashi, T. Ikura, N. Ito, M. Makishima, H. Tokiwa, H. F. DeLuca, et al. 2008. Crystal structures of rat vitamin D receptor bound to adamantyl vitamin D analogs: structural basis for vitamin D receptor antagonism and partial agonism. *J. Med. Chem.* **51**: 5320–5329.
  33. Pace, C. N., F. Vajdos, L. Fee, G. Grimsley, and T. Gray. 1995. How to measure and predict the molar absorption coefficient of a protein. *Protein Sci.* **4**: 2411–2423.
  34. Brunger, A. T., P. D. Adams, G. M. Clore, W. L. DeLano, P. Gros, R. W. Grosse-Kunstleve, J. S. Jiang, J. Kuszewski, M. Nilges, N. S. Pannu, et al. 1998. Crystallography & NMR system: a new software suite for macromolecular structure determination. *Acta Crystallogr. D Biol. Crystallogr.* **54**: 905–921.
  35. McRee, D. E. 1999. XtalView/Xfit—a versatile program for manipulating atomic coordinates and electron density. *J. Struct. Biol.* **125**: 156–165.
  36. Mi, L. Z., S. Devarakonda, J. M. Harp, Q. Han, R. Pellicciari, T. M. Willson, S. Khorasanizadeh, and F. Rastinejad. 2003. Structural basis for bile acid binding and activation of the nuclear receptor FXR. *Mol. Cell.* **11**: 1093–1100.
  37. Inaba, Y., M. Nakabayashi, T. Itoh, N. Yoshimoto, T. Ikura, N. Ito, M. Shimizu, and K. Yamamoto. 2010. 22S-butyl-1 $\alpha$ ,24R-dihydroxyvitamin D<sub>3</sub>: recovery of vitamin D receptor agonistic activity. *J. Steroid Biochem. Mol. Biol.* **121**: 146–150.
  38. Sato, H., A. Macchiarulo, C. Thomas, A. Gioiello, M. Une, A. F. Hofmann, R. Saladin, K. Schoonjans, R. Pellicciari, and J. Auwerx. 2008. Novel potent and selective bile acid derivatives as TGR5 agonists: biological screening, structure-activity relationships, and molecular modeling studies. *J. Med. Chem.* **51**: 1831–1841.



# Peptidyl-prolyl isomerase activity of FK506 binding protein 12 prevents tau peptide from aggregating

Teikichi Ikura<sup>1</sup> and Nobutoshi Ito

Laboratory of Structural Biology, Medical Research Institute, Tokyo Medical and Dental University, 1-5-45 Yushima, Bunkyo-ku, Tokyo 113-8510, Japan

<sup>1</sup>To whom correspondence should be addressed.  
E-mail: ikura.str@tmd.ac.jpReceived May 8, 2013; revised June 6, 2013;  
accepted June 16, 2013

Edited by Haruki Nakamura

The Alzheimer's disease-related protein, tau, aggregates into neurofibrillary tangles when it is hyperphosphorylated. The amino acid sequence included in the third repeat (R3) of the microtubule-binding region is suspected to be the main factor for tau aggregation. Here, we synthesized a 31-residue oligopeptide, corresponding to the R3 region, and characterized its aggregation propensity under various conditions. This peptide aggregated even in the absence of an aggregation-inducing molecule at a low salt concentration, while it did not form any aggregates at a high salt concentration. This suggests that hydrophilic interactions are the main cause of aggregation. We then investigated the function of FK506-binding protein (FKBP) 12, which is known to accumulate in neurofibrillary tangles *in vivo*, on aggregation of the R3 peptide and found that FKBP12 completely prevented the peptide from aggregating at a concentration ratio of 1 : 4 (peptide:FKBP12). FKBP12 also restored the oligomer of the peptide to its monomeric status. Mutational studies on the catalytic center of FKBP12 indicated that peptidyl-prolyl isomerase activity of FKBP12 was essential for prevention of aggregation. Assuming that the propensity of aggregation of the peptide is different in each *cis*-/*trans*-isomer, we propose that the aggregation behavior of the R3 peptide can be theoretically described with a simple kinetic scheme, in which only the *cis*-isomer can aggregate and FKBP12 catalyzes isomerization of the peptide in both the monomeric and aggregative states.

**Keywords:** Alzheimer's disease/FK506 binding protein 12/ neurofibrillary tangles/peptidyl-prolyl isomerase activity/tau protein

## Introduction

The tau protein is essential for assembly and stability of microtubule, which mainly consists of two types of tubulin (Weingarten *et al.*, 1975; Lindwall and Cole, 1984). Hyperphosphorylation of tau abolishes its ability to bind to tubulin and promote microtubule assembly (Bramblett *et al.*, 1993; Yoshida and Ihara, 1993). When it is released from tubulin, phosphorylated tau protein aggregates into neurofibrillary tangles (NFTs), which are the neuropathological hallmarks of Alzheimer's disease (AD) (Goedert *et al.*, 1988; Morishima-Kawashima *et al.*, 1995). Perez *et al.* (2001)

showed that the microtubule-binding domain (MBD) of tau protein is involved in the core of NFT (Fig. 1). The ability to aggregate, however, was impaired in a variant of 3-repeat isoforms of tau protein, which lacked six residues Val306-Gln307-Ile308-Val309-Tyr310-Lys311, in the third region (R3), even though it was hyperphosphorylated. This suggests that the main factor for aggregation of tau protein is included in R3 (Perez *et al.*, 2007).

Dissection analysis was carried out for the MBD. Peptides corresponding to each of the four regions of the MBD (R1, R2, R3 and R4) and various combinations of these (R1–R3, R2–R3, R3–R4, R1–R2–R3, R1–R2–R3–R4 etc.) were chemically synthesized, and their aggregations were investigated by fluorescence-coupled circular dichroism and dynamic light scattering (Mizushima *et al.*, 2006; Zhou *et al.*, 2006; Sugino *et al.*, 2009). Only the peptides including R2 and/or R3 formed filaments in the presence of heparin, although their aggregation processes differed from each other.

A study in 1997 found that a peptidyl-prolyl isomerase (PPIase), Pin1, which specifically isomerized phosphorylated serine or threonine preceding a proline (pSer/Thr-Pro), restored the function of Alzheimer-associated phosphorylated tau protein (Yaffe, 1997; Lu *et al.*, 1999). Pin1 catalyzed prolyl isomerization of specific pSer/Thr-Pro motifs in tau protein to facilitate their dephosphorylation by a Pro-directed phosphatase, PP2A, which was conformation-specific and effectively dephosphorylated only the *trans*-pSer/Thr-Pro isomer (Zhou *et al.*, 2000). A high aggregation-prone (*cis*) isomer was converted to a low aggregation-prone (*trans*) isomer by PPIase activity of Pin1 (Nakamura *et al.*, 2012). As a result, the dephosphorylated tau protein regained ability for assembly and stability of microtubule (Zhou *et al.*, 2000). Phosphorylated sites were mapped on the sequences of various isoforms of tau protein (Brion *et al.*, 1993; Goedert *et al.*, 1993; Kopke *et al.*, 1993; Morishima-Kawashima *et al.*, 1995; Liu *et al.*, 2007). Pin1 worked on several specific sites of at least 30 phosphorylated sites (Lu *et al.*, 1999; Hamdane *et al.*, 2002; Smet *et al.*, 2004; Hamdane *et al.*, 2006; Landrieu *et al.*, 2010; Ogawa *et al.*, 2010). Phosphorylated Thr231-Pro232 was identified as the major target of Pin1 (Lu *et al.*, 1999; Zhou *et al.*, 2000; Nakamura *et al.*, 2012). No pSer/Thr-Pro motif, however, exists on the MBD, indicating that Pin1 does not directly affect the highest aggregation region of tau protein.

Recently, FK506-binding protein (FKBP) 12, FKBP51 and FKBP52 were found to bind to tau (Cao and Konsolaki, 2011). FKBP51 and FKBP52 are PPIases bound to FK506 and rapamycin (Siekierka *et al.*, 1989), and they generally show much higher PPIase activity on Xaa-Pro (Xaa; a standard amino acid residue) motifs than on pSer/Thr-Pro motif (Yaffe, 1997). Both of the large FKBP51 (51 kDa) and FKBP52 (52 kDa), are involved in tau turnover (Chambraud *et al.*, 2010; Jinwal *et al.*, 2010). Although FKBP51 and FKBP52 have very similar structure and both are mostly ubiquitously expressed, these proteins exert opposite effects on tau protein. FKBP51 promotes the association of tau protein with Hsp90, leading to



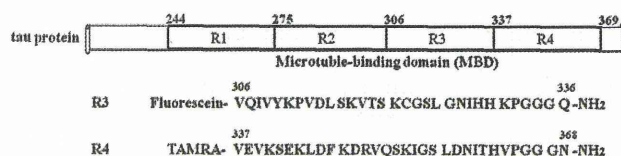


**Fig. 1.** Schematic diagram of four repeat regions in the microtubule-binding domain (MBD) of tau protein and amino acid sequences of the third and fourth repeats (R3 and R4). Labeled fluorophores used in the present study are also shown to the left of the sequences.

dephosphorylation and proper recycling of tau protein (Jinwal *et al.*, 2010), whereas FKBP52 binds directly and specifically to tau protein, preventing tau protein from binding to tubulin (Chambraud *et al.*, 2010). On the other hand, the smaller FKBP12 (12 kDa) co-localized with NFT in AD brains, suggesting that FKBP12 interacted with abnormal forms of tau protein (Harding *et al.*, 1989; Sugata *et al.*, 2009). It is possible that FKBP12 interacts with the MBD of tau protein because the MBD contains eight Xaa-Pro motifs. Assuming each *cis*-/*trans*-isomer of the Xaa-Pro motif in the MBD corresponds with the normal or abnormal form of tau, as seen for phosphorylated Thr231-Pro232, FKBP12 might be able to restore abnormal forms of tau protein to its normal forms. Thus, FKBP12 is a candidate to regulate tau protein by interacting with its MBD.

Here, we synthesized a peptide that corresponds to the R3 region of tau protein (R3 peptide) and investigated whether or not FKBP12 prevents its aggregation *in vitro* under various conditions by fluorescence and dynamic light scattering measurements. In the present study, we focused on the early stage of aggregation of the R3 peptide because Pin1 affected tau protein at the early stage of aggregation (Ramakrishnan *et al.*, 2003; Nakamura *et al.*, 2012). The early stage of aggregation, however, is poorly understood, particularly because of the difficulty of its detection. Thus, we labeled the R3 peptide with fluorescein to increase sensitivity. First, we checked if fluorescein did not change the nature of the peptide with respect to aggregation and investigated the aggregation mechanism for the R3 peptide by measuring aggregation under various conditions. We then measured the aggregation of the R3 peptide in the presence of FKBP12 in order to investigate the aggregation inhibitory activity of FKBP12. As a result, higher the concentration of FKBP12 became, less the aggregation of the R3 peptides was detected. Next, we investigated the aggregation inhibitory mechanism by FKBP12 by introducing two types of mutations Val55 → Arg and Tyr82 → Lys. The former mutation increased the activity 11-fold, whereas the latter decreased it 7-fold. We globally analyzed the relationship between the PPIase activity of FKBP12 and the aggregation inhibitory activity. On the basis of these results, we concluded that the PPIase activity of FKBP12 prevented the R3 peptide from aggregating.

## Materials and methods

### Chemicals

Heparin sodium was of Wako Special Grade from Wako Pure Chemical Industries Ltd. All other chemicals were of guaranteed reagent grade.

### Peptides and proteins

The R3 and R4 peptides, the sequences of which are shown in Fig. 1, were chemically synthesized using a solid-phase peptide synthesizer (Sigma Aldrich Japan K.K.). A fluorescein and an amide group were attached to the N-terminal amide group of Val1 and the C-terminal carboxyl group of Glu31 in the R3 peptide, respectively. TAMRA and amide group were attached to the N-terminal amide group of Val1 and the C-terminal carboxyl group of Asn32 in the R4 peptide, respectively. Their purity was 94.4 and 98.7% for the R3 and R4 peptides, respectively, as determined by mass spectrometry. These peptides were obtained in lyophilized form.

Wild-type human FKBP12 and its two mutants, FKBP12/Val55Arg and FKBP12/Tyr82Lys, were expressed and purified as described previously (Ikura and Ito, 2007).

### Time-dependent fluorescence measurement

Aggregation of the R3 peptide quenched the fluorescence of fluorescein attached to the peptide; as the peptide became more aggregated, the change in fluorescence intensity became larger, as shown in Fig. 2a. Therefore, time-dependent change in fluorescence intensity by fluorescein was measured by a JASCO FP-6500 spectrofluorometer to monitor the time-course of aggregation of the R3 peptide. The excitation and emission wavelengths were 450 and 520 nm, respectively. Before measurements were taken, 1500  $\mu$ l of each buffer solution including salt, heparin, reducing agent or FKBP12, was pre-incubated at 25°C in a rectangular optical cell settled in a Peltier thermostatted cell holder with a magnetic stirrer. Aggregation of the R3 peptide was initiated by diluting 1.5  $\mu$ l of 5 mM (or 15  $\mu$ l of 0.5 mM) of the R3 peptide dissolved in 100% dimethyl sulfoxide (DMSO) in the optical cell. Fluorescence intensity was recorded with time intervals from 5 min to 4–60 h after mixing the peptide. On the other hand, we measured time-dependent change in fluorescence intensity by TAMRA to monitor time-course of aggregation of the R4 peptide as a control experiment. The excitation and emission wavelengths were 500 and 575 nm, respectively. The other experimental conditions and procedures for the R4 peptide were the same as those for the R3 peptide.

### Fluorescence depolarization measurements

The fluorescence depolarization of fluorescein attached to the R3 peptide was measured by the Peltier thermostatted depolarization accessory settled on JASCO FP-6500 spectrofluorometer to investigate the interaction between the R3 peptide and FKBP12 (Weber, 1953; Lakowicz, 1983). The excitation and emission wavelengths were 450 and 520 nm, respectively. Before measurements, 1500  $\mu$ l of each buffer solution including appropriate amount of FKBP12 was pre-incubated at 25°C in a rectangular optical cell settled in the Peltier thermostatted cell holder with a magnetic stirrer. Then, 3  $\mu$ l of 0.5 mM of the R3 peptide solved in 100% DMSO was diluted in the solution. The final concentration of the peptide was set to 1  $\mu$ M, because aggregation of the peptide was not detected at this concentration. Fluorescence depolarization was measured at least 20 times for each condition, and then averaged. These measurements gave apparent dissociation constants ( $K_d$ ) averaged for both of the *cis*- and *trans*-isomers.



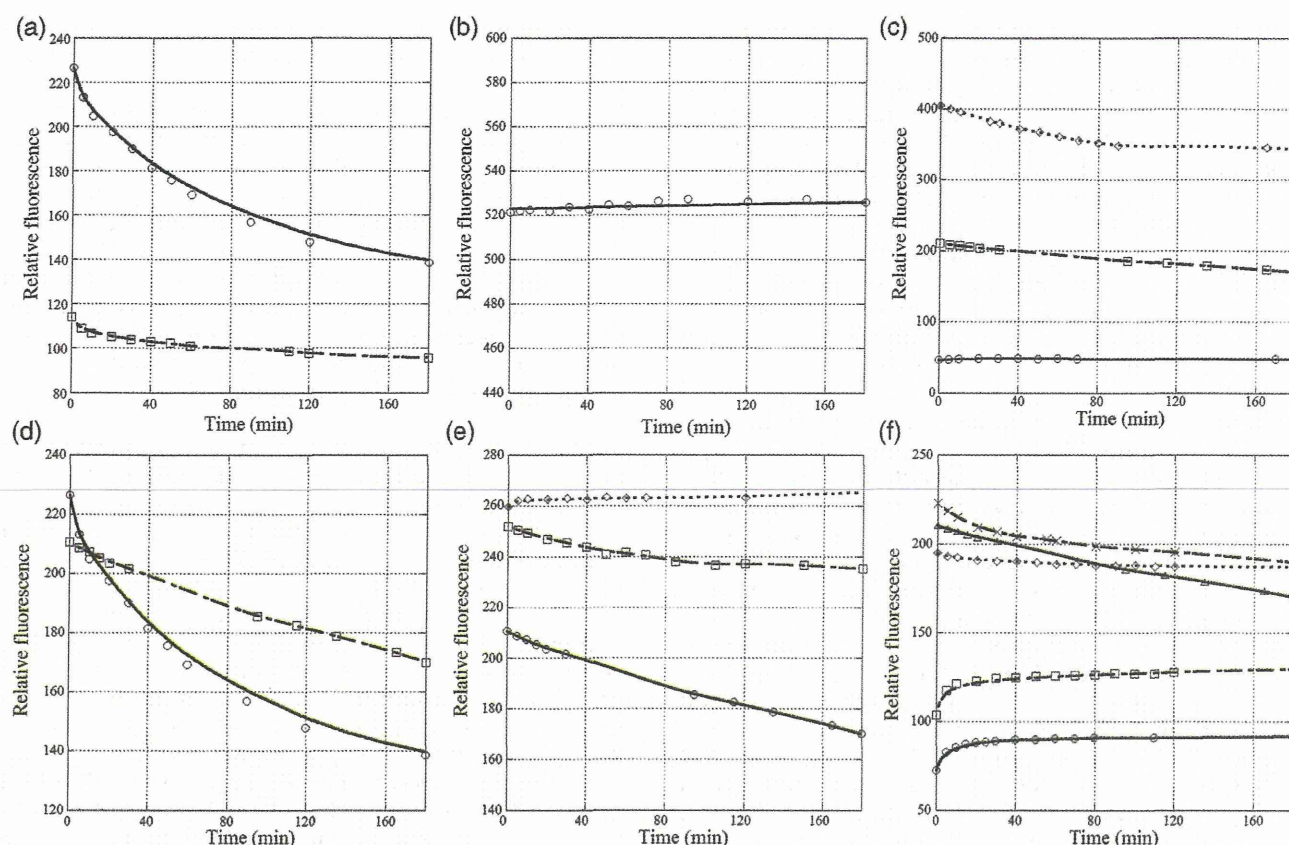


**Fig. 2.** Aggregation of the R3 and R4 peptides under various conditions. Aggregation of the R3 and R4 peptides was monitored in 50 mM sodium phosphate buffer at 25°C with the relative fluorescence of fluorescein and TAMRA attached to the N-terminal amide group of the peptides, respectively. The reaction was started by diluting a 5-mM stock solution of the peptides 1000 times. The other conditions are described in each panel. (a) The aggregation of 5 μM of the R3 peptide at pH 8.0 in the absence (empty circle) and presence (empty square) of 60 μg/mL heparin. (b) The aggregation of the R4 peptide in the absence of heparin. (c) The aggregation of 1 μM (empty circle), 5 μM (empty square) and 10 μM (empty rhombus) of the R3 peptide at pH 8.0 in the presence of 10 mM tris-(2-carboxyethyl)-phosphine hydrochloride (TCEP). (d) The aggregation of 5 μM of the R3 peptide at pH 8.0 in the absence (empty circle) and presence (empty square) of 10 mM TCEP. (e) The aggregation of 5 μM of the R3 peptide at pH 8.0 in the presence of 10 mM TCEP, and in 0 (empty circle), 100 (empty square) or 400 (empty rhombus) mM sodium chloride. (f) The aggregation of 5 μM of the R3 peptide in the presence of 10 mM TCEP, and at pH 4.5 (empty circle), 5.9 (empty square), 6.9 (empty rhombus), 8.0 (empty triangle) or 9.4 (multiplication sign). The aggregation of 5 μM of the R3 peptide at pH 8.0 in the presence of 10 mM TCEP was redundantly plotted in the panels (c), (d), (e) and (f) as a control data. The curve fitting was performed by applying a Stineman interpolating function to the data on KaleidaGraph (Hukinks).

### Dynamic light scattering measurement

Aggregation of the R3 and R4 peptides were directly monitored at 25°C by dynamic light scattering method using Marvern Zetasizer μV. During aggregation measurement, we collected 4 μl of the reaction mixture at hourly intervals and measured ingredient size in the mixture by a laser beam of 830 nm at an angle of 90°.

### Numerical analysis

Numerical analyses were performed using the Mathematica 9.0 software package (Wolfram Res.).

## Results

### Characterization of the R3 peptide's aggregation

To characterize aggregation of the R3 region of tau protein, we chemically synthesized the R3 peptide, the N-terminal valine of which was labeled with fluorescein (Fig. 1), and investigated its aggregation under various conditions by change in the fluorescence intensity of fluorescein. Aggregation of tau

protein and peptides has been conventionally monitored with thioflavin-S (ThS), which quantitatively associates with their aggregated forms. However, it was recently revealed that ThS itself increased the amount of aggregation of tau protein (Carlson *et al.*, 2007; Perez *et al.*, 2007). Thus, we directly labeled the tau peptide with fluorescein to monitor its aggregation in order to exclude ThS-induced artifacts.

**Inducer.** Polyanionic compounds, such as heparin, are well known as *in vitro* inducers for aggregation of the R3 peptide, as well as the tau protein, although the physiological inducer for NFT is not known (Carlson *et al.*, 2007). Initially, we determined whether or not heparin had a similar effect on aggregation of the labeled R3 peptide, because no experimental data have been reported for the labeled R3 peptide (Fig. 2a). As reported for the non-labeled peptides (Mizushima *et al.*, 2006), 5 μM of the labeled R3 peptide rapidly aggregated in the presence of 60 μg/ml of heparin, and then its aggregates gradually grew into larger particles. We also found that the peptide aggregated at this concentration even in the absence of heparin (Fig. 2a). The aggregation in the absence of heparin,



however, grew much slower than that in the presence of heparin. The sizes of the aggregated particles were measured by the dynamic light scattering method; after 20 min, the aggregations grew into large particles with mean hydrodynamic radii of  $206.8 \pm 130.6$  and  $16.30 \pm 8.97$  nm in the presence and absence of heparin, respectively. These aggregations were still soluble in the aqueous solution at that time, but precipitated within 60 h. In contrast, the labeled R4 peptide did not aggregate under the same condition (Fig. 2b), as reported by Mizushima *et al.* (2006). These results indicate that the R3 peptide intrinsically has a high propensity to aggregate. Heparin was not necessary for the R3 peptide to aggregate, but it enhanced aggregation of the R3 peptide.

**Saturation point.** What is the minimum concentration (saturation point) for the R3 peptide to aggregate? In general, proteins have higher aggregation propensities at lower saturation points. Is this general property true for the R3 peptide? To answer this question, we investigated aggregation of the R3 peptide at three different concentrations, 1, 5 and 10  $\mu$ M, to elucidate its concentration-dependence in aggregation, in the absence of any inducer. Figure 2c shows that 5 and 10  $\mu$ M of the peptide formed aggregates, whereas 1  $\mu$ M of the peptide did not. These results indicate that the saturation point of the R3 peptide is between 1 and 5  $\mu$ M in the absence of heparin. This value is similar to the saturation point for the intact tau protein observed in the presence of heparin (Carlson *et al.*, 2007). This, however, seems quite high in contrast with the  $\alpha$ -amyloid (1–40) peptide, which aggregates at 40 nM under a specific condition (Ding *et al.*, 2012). Thus, the tau protein may be rather soluble among proteins forming amyloid-like fibers.

**Oxidation.** The tau protein isoforms have, at most, two cysteine residues. For example, the N2R4 isoform (441 amino acid residues) contains Cys291 and Cys322. Both cysteine residues are located in the MBD, Cys291 in the R2 region, and Cys322 in the R3 region. These cysteine residues formed intramolecular and intermolecular disulfide bonds and accelerated the aggregation of tau peptides (Sugino *et al.*, 2009). In the present study, only one cysteine residue, Cys322 (Cys17 in the R3 peptide's sequence), was included in the R3 peptide, suggesting that it was able to dimerize the peptide under oxidative conditions. Thus, we investigated how the oxidation of Cys17 affected the aggregation of the R3 peptide. Figure 2d shows that the R3 peptide aggregated much faster under the oxidative condition than under the reductive condition, suggesting that dimerization of the R3 peptide accelerates the aggregation. According to Sugino *et al.* (2009), two types of tau peptides, 4RMDB (R1–R2–R3–R4) and 3RMDB (R1–R3–R4), formed homodimers, with an intramolecular and intermolecular disulfide bond, respectively. After dimerization, the peptides assemble into large aggregations, depending on their sequences. The R3 peptide also aggregated under the oxidative condition, and the aggregation rate was almost the same as that of the rate of 3RMDB. Thus, the mechanism of aggregation of the R3 peptide was expected to be the same as that of 3RMDB, although they did not specifically mention it (Sugino *et al.*, 2009). The disulfide bonds, however, were not essential for the aggregation of tau peptides, including R3, 3RMDB and 4RMDB. These tau peptides aggregated, even under the reductive condition (Fig. 2d) (Sugino *et al.*, 2009), suggesting that

the aggregation mechanism under the reductive condition was different from the mechanism under the oxidative condition.

**Salt effect.** As shown above, heparin accelerated aggregation of the R3 peptide (Fig. 2a), suggesting that the aggregation of the peptide was driven mainly by hydrophilic interactions. Here, we measured the aggregation of the R3 peptide under various salt concentrations in the presence of the reductant to elucidate the charge effect on the aggregation. Figure 2e shows that the aggregation of the R3 peptide decreased when the salt concentration increased. The R3 peptide did not aggregate in the presence of 400 mM of sodium chloride. This result also indicated that the hydrophilic interactions affect the aggregation of the R3 peptide considerably.

**pH dependency.** We next investigated the type of hydrophilic amino acid residues responsible for aggregation of the R3 peptide. The R3 peptide includes eight hydrophilic residues, one aspartic acid residue, two histidine residues, four lysine residues and one tyrosine residue. Thus, we measured the aggregation of the R3 peptide at five different pHs, 4.5, 5.9, 6.9, 8.0 and 9.4, in the presence of reductant. The electrostatic interaction of the R3 peptide almost vanished at pH 9.4, because the isoelectric point of the R3 peptide is theoretically 9.98. This suggests that the hydrophobic effects were greatest at pH 9.4. In contrast, lower the pH becomes, more positive the net charge of the R3 peptide becomes. This suggests that the hydrophilic effects become the largest at pH 5.9. At the mid-range pHs, both the hydrophilic and hydrophobic effects were medium, but distribution of the local charge of the R3 peptide was dependent on the pH. We found that aggregation of the R3 peptide was at the minimum and maximum levels at pH 6.9 and 8.0, respectively (Fig. 2f), suggesting that the distribution of the local charge was more important for aggregation of the R3 peptide than the net charge of the peptide. Furthermore, the transition to aggregation of the R3 peptide occurred between pH 6.9 and 8.0, suggesting that distribution of the local charge of the peptide changed between pH 6.9 and 8.0. One of the candidate mechanisms for changing the charge is deprotonation of the histidine residue. The R3 peptide contains two histidine residues, His24 and His25. The local positive charge around the histidine residues might be related to aggregation of the R3 peptide.

In summary, the R3 peptide aggregated even in the absence of inducer, and the aggregation was driven by hydrophilic interaction. The deprotonation of histidine seemed to affect aggregation of the peptide.

#### Aggregation inhibition by FKBP12

The R3 peptide contains two proline residues, Pro7 and Pro27. The proline residues are not the target for Pin1 but are the targets for FKBP12, because Lys6 and Lys26 precede the proline residues (Yaffe, 1997). In order to elucidate the aggregation inhibitory activity of FKBP12, we measured aggregation of the R3 peptide in various concentrations of FKBP12 by change of fluorescence intensity of fluorescein. Figure 3a shows that R3 peptide aggregation decreased when the concentration of FKBP12 increased. No peptide aggregation was detected in the presence of 20  $\mu$ M of FKBP12. This result clearly indicated that FKBP12 prevents the R3 peptide from aggregating. We calculated that 50% inhibitory concentration ( $IC_{50}$ ) of FKBP12 under the conditions was 3  $\mu$ M (Fig. 3b).



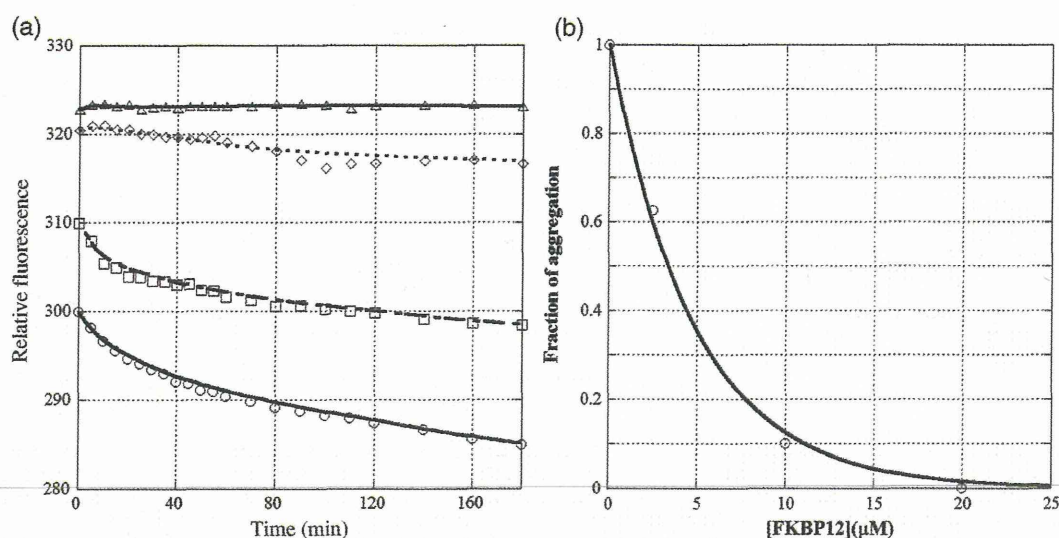
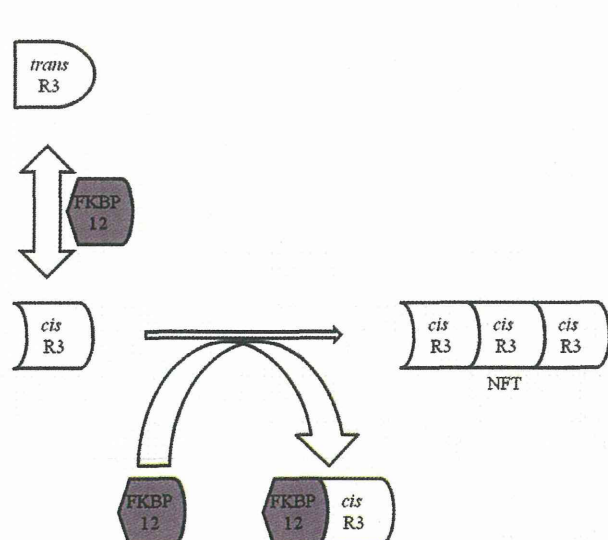
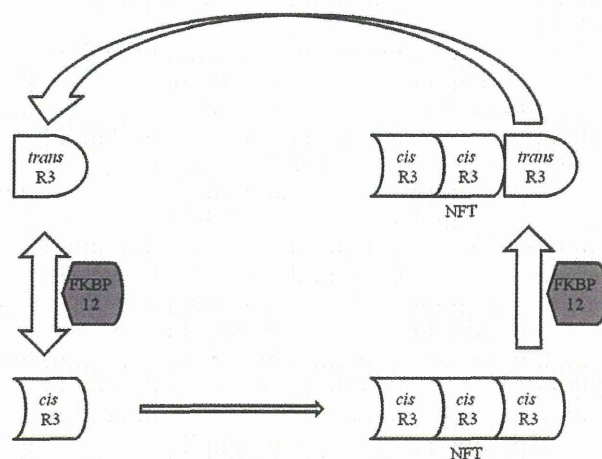


**Fig. 3.** (a) Aggregation of the R3 peptides in the presence of FKBP12. The aggregation of 5  $\mu\text{M}$  of the R3 peptide was monitored in the presence of 0 (empty circle), 2.5 (empty square), 10 (empty rhombus) or 20 (empty triangle)  $\mu\text{M}$  FKBP12 at pH 8.0 and 25°C with the relative fluorescence of fluorescein. The reaction started by diluting 0.5-mM stock solution of the peptide 100 times. The reaction mixture also contained 50 mM sodium phosphate and 10 mM TCEP. Curve fitting was performed by applying a Stineman interpolating function to the data on KaleidaGraph (Hukinks). (b) The normalized amount of aggregation in the presence of FKBP12. The normalized amount of aggregation was calculated by dividing the decrease in fluorescence during the first 180 min by the decrease in the absence of FKBP12. Curve fitting was based on the two-state transition theory. The 50% inhibitory concentration ( $\text{IC}_{50}$ ) of FKBP12 was calculated at 3  $\mu\text{M}$  on the basis of this graph.



**Scheme 1.** The inhibitory mechanism of R3 peptide aggregation by simple binding of FKBP12. In this scheme, only the *cis*-isomer of the R3 peptide can aggregate, to which FKBP12 specifically and tightly binds. FKBP12 catalyzes isomerization of Xaa-Pro motifs of the R3 peptide only in the monomeric state. Association between FKBP12 and the *cis*-isomer is much faster than self-association of the *cis*-isomer because the concentration of the *cis*-isomer is very low. Therefore, FKBP12 intercepts the *cis*-isomer during its aggregation.

There are two possible explanations for the mechanism of how FKBP12 prevents the R3 peptide from aggregating (Schemes 1 and 2). One is that FKBP12 sequesters the R3 peptide: (i) FKBP12 tightly binds to the R3 peptide, (ii) the effective concentration of the R3 peptide decreases to less than its saturation point and (iii) FKBP12 also interacts with oligomers of the R3 peptide at the early stage of aggregation,



**Scheme 2.** The inhibitory mechanism of R3 peptide aggregation by PPIase activity of FKBP12. In this scheme, only the *cis*-isomer of the R3 peptide can aggregate, and FKBP12 does not tightly bind to either isomer. FKBP12 catalyzes isomerization of Xaa-Pro motifs of the R3 peptide in both the monomeric and aggregative state. Once the *cis*-isomer is converted into the *trans*-isomer in the aggregative state, the *trans*-isomer is quickly released from the aggregation because the *trans*-isomer cannot aggregate.

leading to dissociation of the peptide (Scheme 1). The other possible explanation is that FKBP12 catalyzes isomerization from the higher aggregation-prone isomer to the lower one: (i) FKBP12 binds more tightly to the higher aggregation-prone isomer of the R3 peptide than to the lower one, and (ii) FKBP12 catalyzes isomerization from the higher aggregation-prone isomer to the lower one as well as Pin1 and (iii) FKBP12 also functions for oligomers of the R3 peptide at the early stage of aggregation, leading to dissociation of the peptide (Scheme 2). Both schemes have the association of FKBP12 with the R3 peptide in common. However, they are



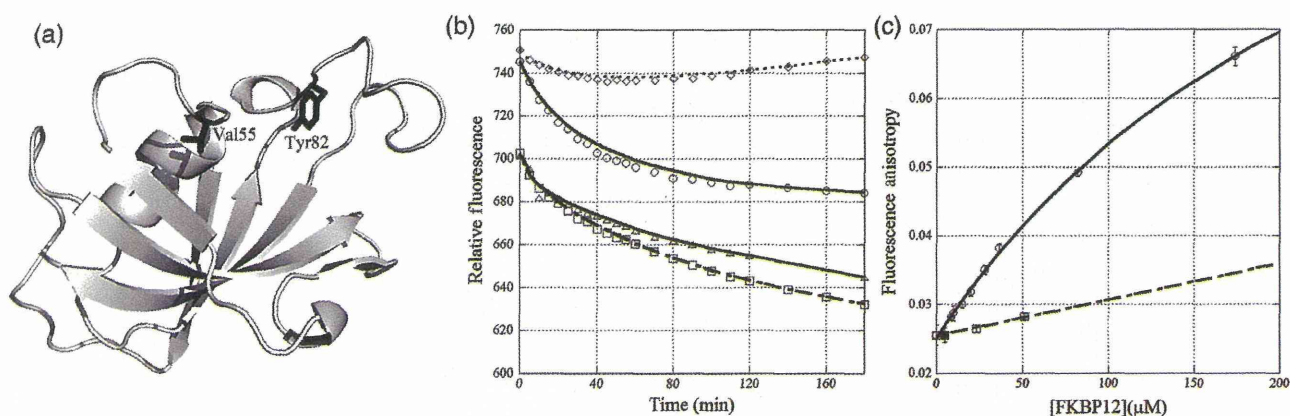


**Fig. 4.** (a) The positions of mutations on the tertiary structure of FKBP12. The two residues are drawn with a stick model. (b) Aggregation of 5  $\mu\text{M}$  of the R3 peptides in the presence of 5  $\mu\text{M}$  wild-type FKBP12 (empty circle), 5  $\mu\text{M}$  FKBP12/Tyr82Lys (empty square) and 5  $\mu\text{M}$  FKBP12/Val55Arg (empty rhombus), and in the absence of FKBP12 (empty triangle). The other conditions are the same as described in Fig. 3. Curve fitting was performed by applying a Stineman interpolating function to the data on KaleidaGraph (Hukinks). (c) Fluorescence depolarization of fluorescein attached to the R3 peptide for titration of wild-type FKBP12 (empty circle), FKBP12/Tyr82Lys (empty square) and FKBP12/Val55Arg (filled square). The concentration of R3 peptide needed to prevent aggregation was 1  $\mu\text{M}$ . Curve fitting was based on the two-state transition theory. The dissociation constant ( $K_d$ ) for wild-type FKBP12 was calculated at 271  $\mu\text{M}$ . The  $K_d$  values for the mutant proteins could not be determined because of the very weak interaction between the peptide and the mutant proteins.

different in the catalytic reaction of FKBP12. FKBP12 only sequesters the peptide in the former scheme, while it catalyzes the isomerization of Xaa-Pro bonds of the peptide in the latter scheme.

To determine which scheme is applicable to the function of FKBP12, we introduced two types of mutations into FKBP12; one mutation increased the PPIase activity, and the other mutation decreased the activity. A Val55  $\rightarrow$  Arg mutation (FKBP12/Val55Arg) increased PPIase activity by a factor of 11, while a Tyr82  $\rightarrow$  Lys mutation (FKBP12/Tyr82Lys) decreased the activity by a factor of 7 (Fig. 4a) (Ikura and Ito, 2007). In order to elucidate the effect of PPIase activity, we measured the aggregation of 5  $\mu\text{M}$  of the R3 peptide in the presence of 5  $\mu\text{M}$  of each of these mutant proteins by change in fluorescence intensity of fluorescein. Moreover, in order to elucidate how the mutations affect the association between FKBP12 and the R3 peptide, we measured the affinities of the proteins to the R3 peptide by the fluorescence depolarization method. In this affinity study, concentration of the R3 peptide was decreased to 1  $\mu\text{M}$  because the R3 peptide did not aggregate at this concentration (Fig. 2c). As the results indicated, the R3 peptide did not aggregate in the presence of FKBP12/Val55Arg, while FKBP12/Tyr82Lys did not inhibit the aggregation (Fig. 4b). In the presence of FKBP12/Val55Arg, the R3 peptide aggregated transiently at first, then gradually dissociated and finally, the peptide was completely restored from the aggregation. The apparent dissociation constant ( $K_d$ ) for wild-type FKBP12 was calculated as 271  $\mu\text{M}$ , whereas the  $K_d$ s for each of the two mutants was much  $>271 \mu\text{M}$  (Fig. 4c). These affinities were too low for  $K_d$  calculation by the fluorescence depolarization method. These results indicated that higher the PPIase activity of FKBP12, higher its aggregation inhibitory activity. The results also indicated that the aggregation inhibitory activity of FKBP12 was independent of the affinity between FKBP12 and the R3 peptide. Therefore, the aggregation inhibitory activity of FKBP12 depended only on the PPIase activity of FKBP12, as represented by Scheme 2.

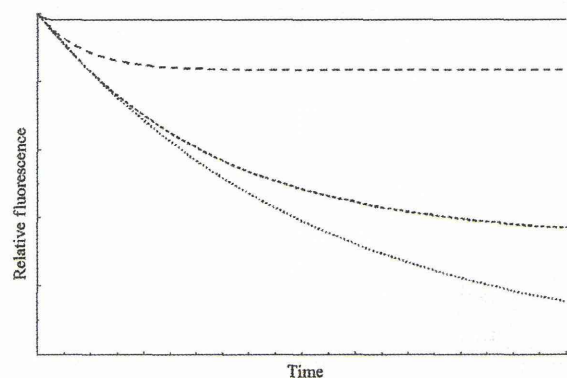


**Fig. 5.** Theoretical analysis of the aggregation of the R3 peptide in the presence of FKBP12. Each curve was calculated by numerically solving the differential equations derived from Scheme 2. The solid and dotted lines indicate the highest and lowest concentrations of FKBP12, respectively. Two dashed lines represent the mid-level concentration of FKBP12. This figure reflects Fig. 3 as well, indicating that Scheme 2 is a good descriptor of the function of FKBP12.

## Discussions

### Mechanism of FKBP12 inhibition of R3 peptide aggregation

As shown in Fig. 3a, 20  $\mu\text{M}$  of FKBP12 completely inhibited aggregation of the R3 peptide. Mutational studies on FKBP12 showed that the aggregation inhibitory activity of FKBP12 is attributable mainly to its PPIase activity (Fig. 4b and c). Furthermore, FKBP12 not only acted on the R3 peptide in the monomeric state but also in the aggregative state (Fig. 4a). This restoration of the R3 peptide from aggregate to monomer suggests that the R3 peptide aggregation formed at the early stage does not strongly resist the attack by FKBP12. These features of the aggregation of the R3 peptide in the presence of FKBP12 are well described in Scheme 2. On the other hand, the mutational studies showed that the aggregation inhibitory mechanism of FKBP12 was inconsistent with Scheme 1, because the mutation Val55  $\rightarrow$  Arg weakened the association



between FKBP12 and the peptide, but raised the aggregation inhibitory activity (Fig. 4b and c). Here, we theoretically examined how Scheme 2 reproduced the experimental results. In simulating the inhibition of R3 peptide aggregation by FKBP12 in Scheme 2, we simplified the reaction so that (i) only the *cis*-isomer of the Xaa-Pro motif aggregated irreversibly, (ii) FKBP12 accelerated the isomerization between *cis*- and *trans*-isomers in monomeric and aggregative states and (iii) only the *trans*-isomer in the aggregative state quickly dissociated from the aggregation. As a result, the acceleration of isomerization decreased the amount of aggregation of the R3 peptide (Fig. 5), indicating that Scheme 2 describes the experimental results, in which FKBP12 restored the R3 peptide from the aggregation. Although no structural information is available to explain the difference between the *cis*- and *trans*-isomers, we can interpret this issue on the basis of pH dependency of the aggregation (Fig. 2f). Aggregation of the R3 peptide was sensitive to the distribution of local charge. The *cis*- and *trans*-isomers are probably different from each other in the distribution of local charge. Therefore, the *cis*-isomer is much aggregative than the *trans*-isomer, as reported for the aggregation propensity of the pThr231-Pro232 motif (Nakamura *et al.*, 2012).

In 2001, von Bergen *et al.* pointed out that Pro312 was important for aggregation propensity of the R3 peptide (von Bergen *et al.*, 2001). They reported that a deletion mutant of a short R3 peptide (Val306-Lys317), which lacked only Pro312, showed a pronounced shift to  $\beta$ -structure and enhanced the aggregation, indicating that the aggregation propensity of the R3 peptide correlated with the  $\beta$ -structure content for residues around the Val306-Lys311 motif, and Pro312 in the intact sequence broke elongation of  $\beta$ -structure by its restricted conformation. This means that Pro312 suppresses aggregation of the R3 peptide. Although they did not investigate the isomerization of Pro312, this suppressive effect should be brought about by the *trans*-isomer because it is in majority. The *cis*-isomer might have higher  $\beta$ -structure content for the R3 peptide than the *trans*-isomer. Therefore, isomerization of Pro312 presumably attributes to the aggregation propensity of the R3 peptide.

### In vivo function of FKBP12

FKBP12 was first discovered as the receptor for an immunosuppressor in the immune system (Harding *et al.*, 1989; Siekierka *et al.*, 1989). It was later revealed that FKBP12 had multiple functions in cells. FKBP12 interacts with signal transduction proteins such as the type-1 transforming growth factor receptor (Chen *et al.*, 1997), and with multiple intracellular calcium release channels, such as the tetrameric skeletal muscle ryanodine receptor (Gaburjakova *et al.*, 2001). FKBP12 is also abundantly expressed in the brain and accumulates in NFT (Sugata *et al.*, 2009). However, whether or not FKBP12 is concerned with the aggregation process of tau protein was still unclear. In this study, we clearly demonstrated that FKBP12 prevented the R3 peptide from aggregating *in vitro*. Although a short fragment of tau protein, the R3 region was essential for tau protein to aggregate (Perez *et al.*, 2007). Therefore, it is expected that FKBP12 prevents tau protein aggregation by interacting with the R3 region of tau protein *in vivo*, as it acts upon the R3 peptide *in vitro*. In its *in vitro* aggregation inhibitory activity, FKBP12 catalyzed the isomerization both of monomeric and aggregative states, suggesting that

such isomerization catalysis is also essential for its *in vivo* aggregation inhibitory activity.

### PPIase versus NFT

At least four PPIases, Pin1, FKBP12, FKBP51 and FKBP52, are estimated to be responsible for stabilizing and destabilizing the tau protein *in vivo* (Cao and Konsolaki, 2011; Nakamura *et al.*, 2012). Pin1 interacts with the pSer/Thr-Pro motifs in the tau protein and isomerizes the higher aggregative *cis*-isomer to the low aggregative *trans*-isomer. The functions of FKBP51 and FKBP52 are related to association and dissociation between the tau protein and two types of tubulins. However, whether or not the PPIase activities of both FKBP51 and FKBP52 are concerned with the function is unknown, because they consist of several functional domains. On the other hand, this study suggested that PPIase activity of FKBP12 was essential in preventing tau protein aggregation. Thus, many PPIases and their PPIase activities regulate the tau protein. Such a feature of the tau protein might be related to one of its structural properties, in which it is intrinsically disordered (Skrabana *et al.*, 2006).

### Acknowledgements

We thank Professor Nobuhiro Takahashi (Tokyo University of Agriculture and Technology) for providing the cloned gene of human FKBP12.

### Funding

This work was supported by Grants-in-Aid for Scientific Research (No 22113504) from the Ministry of Education, Culture, Sports, Science and Technology of Japan.

### References

- Bramblett, G.T., Goedert, M., Jakes, R., Merrick, S.E., Trojanowski, J.Q. and Lee, V.M. (1993) *Neuron*, **10**, 1089–1099. First published on 1993/06/01.
- Brion, J.P., Smith, C., Couck, A.M., Gallo, J.M. and Anderton, B.H. (1993) *J. Neurochem.*, **61**, 2071–2080. First published on 1993/12/01.
- Cao, W. and Konsolaki, M. (2011) *J. Biosci.*, **36**, 493–498. First published on 2011/07/30.
- Carlson, S.W., Branden, M., Voss, K., Sun, Q., Rankin, C.A. and Gamblin, T.C. (2007) *Biochemistry*, **46**, 8838–8849. First published on 2007/07/05; doi: 10.1021/bi700403a.
- Chambraud, B., Sardin, E., Giustiniani, J., Dounane, O., Schumacher, M., Goedert, M. and Baulieu, E.E. (2010) *Proc. Natl Acad. Sci. USA*, **107**, 2658–2663. First published on 2010/02/06; doi: 10.1073/pnas.0914957107.
- Chen, Y.G., Liu, F. and Massague, J. (1997) *EMBO J.*, **16**, 3866–3876. First published on 1997/07/01; doi: 10.1093/emboj/16.13.3866.
- Ding, H., Schauerte, J.A., Steel, D.G. and Gafni, A. (2012) *Biophys. J.*, **103**, 1500–1509. First published on 2012/10/16; doi: 10.1016/j.bpj.2012.08.051.
- Gaburjakova, M., Gaburjakova, J., Reiken, S., Huang, F., Marx, S.O., Rosembly, N. and Marks, A.R. (2001) *J. Biol. Chem.*, **276**, 16931–16935. First published on 2001/03/30; doi: 10.1074/jbc.M100856200.
- Goedert, M., Wischik, C.M., Crowther, R.A., Walker, J.E. and Klug, A. (1988) *Proc. Natl Acad. Sci. USA*, **85**, 4051–4055. First published on 1988/06/01.
- Goedert, M., Jakes, R., Crowther, R.A., Six, J., Lubke, U., Vandermeeren, M., Cras, P., Trojanowski, J.Q. and Lee, V.M. (1993) *Proc. Natl Acad. Sci. USA*, **90**, 5066–5070. First published on 1993/06/01.
- Hamdane, M., Smet, C., Sambo, A.V., *et al.* (2002) *J. Mol. Neurosci.*, **19**, 275–287. First published on 2003/01/24; doi: 10.1385/JMN:19:3:275.
- Hamdane, M., Dourlen, P., Bretteville, A., *et al.* (2006) *Mol. Cell. Neurosci.*, **32**, 155–160. First published on 2006/05/16; doi: 10.1016/j.mcn.2006.03.006.
- Harding, M.W., Galat, A., Uehling, D.E. and Schreiber, S.L. (1989) *Nature*, **341**, 758–760. First published on 1989/10/26; doi: 10.1038/341758a0.
- Ikura, T. and Ito, N. (2007) *Protein Sci.*, **16**, 2618–2625. First published on 2007/11/22; doi: 10.1110/ps.073203707.
- Jinwal, U.K., Koren, J., III, Borysov, S.I., *et al.* (2010) *J. Neurosci.*, **30**, 591–599. First published on 2010/01/15; doi: 10.1523/JNEUROSCI.4815-09.2010.